Research Article

Plasma Reactor Generating Synchronous Flows of Bactericidal UV Radiation and Nanostructures of Zinc, Copper, Iron Oxides and Chalcopyrite

Shuaibov AK*, Minya AY, Gomoki ZT, Malinina AA, Malinin AN, Danilo VV, Bilak YU and Kolozhvari CH

Faculty of Physics, State Higher Educational Establishment, Uzhgorod National University, Uzhhorod, Ukraine

Abstract

The characteristics of a plasma-chemical reactor based on an overstressed nanosecond discharge in atmospheric pressure gases (air, nitrogen, helium, argon) between electrodes of zinc, copper and iron, as well as of chalcopyrite (CuInSe2) at a distance between the electrodes of 1-3 mm are given. It was established that this discharge is a point source of ultraviolet radiation in the spectral range of 200-300 nm and a flow of transition metal oxide nanoparticles (Zn, Cu, Fe), as well as chalcopyrite nanoparticles. The results of the optimization of a UV emitter depending on the pumping conditions and parameters of the discharge medium, as well as the optical characteristics of film nanostructures of transition metal oxides and chalcopyrite deposited on the surface of a glass substrate, are presented.

Keywords: Air; Chalcopyrite; Copper; Helium; Iron; Overstressed nanosecond discharge; Radiation and Transmission spectrum; Zinc

Introduction

Currently, the use of gas-discharge lamps of ultraviolet radiation in biotechnology, medicine, micro-nanoelectronics and photochemistry is becoming increasingly widespread [1-3]. But other equally important factors of modern biomedical technologies, for example, flows of metal nanoparticles, are also becoming more and more often in demand in modern Technologies of medicine, biology [4,5] and for agricultural production it is important to develop new effective emitters of the visible range of the spectrum to stimulate plant growth in greenhouses [6,7].

The characteristics of a high-current, overstressed nanosecond discharge in the air between copper electrodes and semiconductor electrodes based on the CuInSe$_2$ compound, which are sources of both bactericidal UV radiation in the spectral range 200-230 nm, and the flow of copper oxide and chalcopyrite nanoparticles are given in [8-11]. Nanostructures of metal oxides were deposited from this discharge onto a glass substrate and their optical characteristics were subsequently determined by electron microscopy, absorption-transmission spectroscopy, Raman spectroscopy, and photoluminescence.

Nanostructures based on zinc and copper oxides are characterized by a pronounced antimicrobial effect [12-14].

On this basis, the development of new methods for the simultaneous production of bactericidal ultraviolet radiation and flows of transition metal nanoparticles and chalcopyrite, which will enhance the inactivation and antimicrobial properties of gas-discharge plasma, are of considerable interest for applications in biomedical engineering, including microbiology, medicine, as well as agricultural technologies.

This article presents the main parameters of a high-pressure plasma chemical reactor with an overstressed nanosecond discharge between electrodes of transition metals (Zn, Cu, Fe) and chalcopyrite, its electrical and optical characteristics, the results of modeling plasma parameters, and also the results of a study of the characteristics of nanostructures of transition metal oxides and chalcopyrite films that have been deposited on a glass substrate mounted near an electrode system. The promising areas of application of a plasma reactor in biomedical engineering are briefly reviewed.

Methodology

Technique and experimental conditions

A schematic diagram of a gas-discharge reactor pumped by a nanosecond overstressed discharge of nanosecond duration in atmospheric pressure air, nitrogen, and inert gases (He, Ar) and a device for the synthesis of film nanostructures are presented in figure 1. The cylindrical electrodes of the discharge device had a diameter of 5 mm and a length of 30 mm and were made of zinc, copper, stainless steel and polycrystalline chalcopyrite (CuInSe$_2$). The electrodes were installed in a sealed chamber of a dielectric, which had a volume of 3 liters. The radius of curvature of the working end part of the electrodes was 3 mm. To reduce the influence of electromagnetic interference on the recording system of discharge characteristics, a cell with a system of electrodes was installed in a screen of metal mesh. The discharge for all types of electrodes was studied mainly at buffer gas pressures of 101-202 kPa.
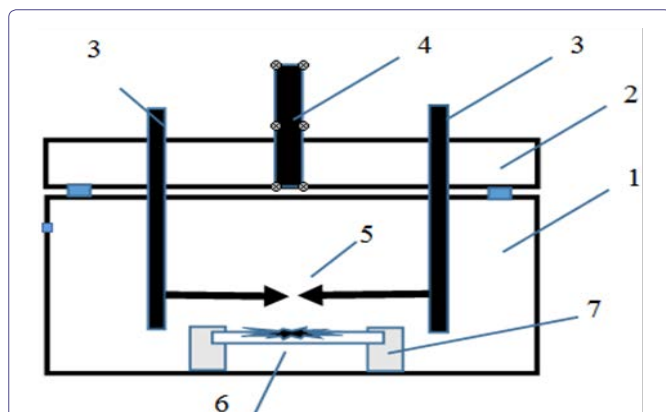
Figure 1: The scheme of the discharge device for the synthesis of chalcopyrite thin films on the surface of glass or quartz: 1:A plexiglas discharge chamber, 2: An upper flange, 3: Hermetic metal leads, 4: A fitting for connecting to a vacuum gas mixing system, 5: Electrodes with chalcopyrite, 6: Glass substrate with a film based on sputtered electrodes, 7: Plate fixing system.

To ignite the discharge, high voltage pulses of positive and negative polarity (bipolar pulses) with a duration of 50-100 ns and an amplitude of up to ± (20-40) kV were applied to the electrodes. In this case, between the tips of the electrodes, a uniform discharge was ignited with amplitude of current pulses of 50-170 A [15]. The volume of the discharge plasma did not exceed 5-10 mm^3. With an interelectrode distance of 1-3 mm, the discharge gap was overstressed. Under such a regime of ignition of the discharge, favorable conditions were created for ecton introduction of vapor of the material of the electrodes from electrodes, as was observed in [16], where copper electrodes were used.

The voltage pulses at the discharge gap and the discharge current were measured using a broadband capacitive divider, Rogowsky coil, and a 6-LOR 04 broadband oscilloscope. The time resolution of this recording system was 2-3 ns. The spatial characteristics of the discharge were studied using a digital camera. The pulse repetition rate varied in the range f = 35-1000 Hz. The plasma radiation spectra were recorded using an MDR-2 monochromator, an FEU-106 photomultiplier, a direct current amplifier, and an electronic potentiometer. The radiation from the discharge plasma was analyzed in the spectral region of 200–650 nm. The total relative power of the discharge UV radiation in the spectral range 200-280 nm was measured using the TKA-PKM ultraviolet radiation power meter. The transmission spectra of the radiation with thin nanostructured films that were deposited on glass substrates were recorded using an OCEAN OPTICS USB 2000 spectrometer. The probe radiation was applied to the film and glass substrate using an optical fiber system.

The transmission spectra of chalcopyrite films were studied using a spectral complex based on an MDR-23 monochromator at room temperature in the wavelength range of 200-850 nm. The technique of such studies is given in [3].

The films were sputtered for 30-60 minutes when a glass substrate was installed at a distance of 30 mm from the center of the discharge gap, an interelectrode distance of 1-3 mm, a voltage pulse amplitude of ± (20-40) kV, and a pulse repetition rate of 40-100 Hz.

The surface image of thin nanostructured films was recorded using a Cross Beam Workstation Auriga scanning electron microscope (Carl Zeis).

The photoluminescence spectra of the synthesized films were studied by irradiating the film with radiation from a high-pressure arc mercury lamp at different wavelengths in the spectral range: 270-600 nm. In this case, the radiation of a mercury lamp in the spectral intervals of 5 nm was allocated within the fixed wavelengths using a separate monochromator and then directed to the film surface. The photoluminescence spectrum of nanostructures was recorded by a separate spectrophotometer.

Results and Discussion

Characteristics and parameters of an overstressed nanosecond discharge

In figure 2 images of an overstressed nanosecond discharge between copper electrodes in atmospheric pressure air at voltage pulse repetition rates of 40-1000 Hz.
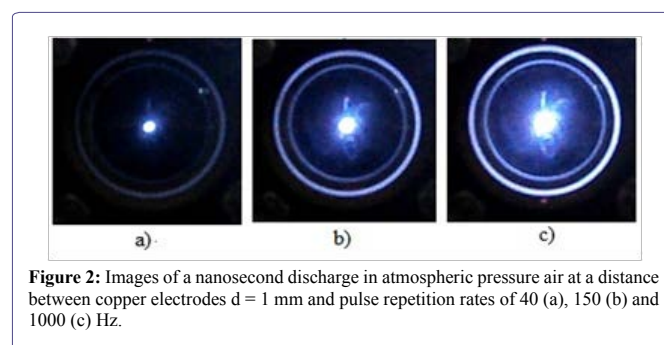
Figure 2: Images of a nanosecond discharge in atmospheric pressure air at a distance between copper electrodes d = 1 mm and pulse repetition rates of 40 (a), 150 (b) and 1000 (c) Hz.

A nanosecond discharge was formed under conditions of a strong overstress of the discharge gap (at d = 1 mm) and with a slightly inhomogeneous distribution of the electric field strength between electrodes with a spherical working surface with rather large round radii (r = 3 mm). The diffuse form and shape of the investigated discharge was close to spherical. At low repetition rates of voltage pulses (f = 40-150 Hz), the diameter of spherical plasma formation was approximately equal to the interelectrode distance, and when the repetition rate increased to 1000 Hz, its diameter increased by 3-4 times. In this case, the Plasma spread to new areas of the surface of the spherical part of the metal electrodes. In such a regime of ignition of the discharge and in the presence of natural micro protrusions on the working surfaces of the electrodes, the latter explode in a strong electric field, which leads to the injection of the electrode material into the plasma and the formation of ectons [16]. Preservation of the spherical form of plasma formation at elevated repetition rates of voltage pulses can be associated with the action of ultraviolet and X-ray radiation, which illuminates the entire discharge gap isotropically [17,18]. The spatial characteristics of the discharge did not change significantly when replacing copper electrodes with electrodes of zinc, stainless steel, and chalcopyrite.

In figure 3 shows characteristic waveforms of the voltage and current of an overstressed nanosecond discharge in air using copper electrodes as an example.
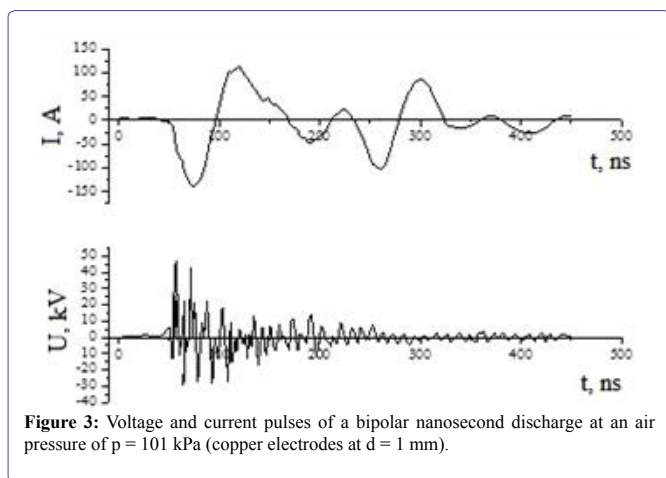
Figure 3: Voltage and current pulses of a bipolar nanosecond discharge at an air pressure of p = 101 kPa (copper electrodes at d = 1 mm).

Similar oscillograms were also obtained for discharges between electrodes of zinc, copper, stainless steel, and chalcopyrite. The duration of the main part of the train of voltage pulses reached 50-120 ns. The bipolar spikes of the voltage pulse had amplitude of the positive and negative component up to 20-40 kV. The discharge current pulses were a sequence of current pulses with amplitude of positive and negative pulses of 120-150 A. The total length of a sequence of current pulses with decreasing amplitude in time reached 150-200 ns.

By graphically multiplying the waveform of the current pulses and the voltage waveform, the time distribution of the pulsed energy contribution to the plasma was obtained. The maximum pulse discharge power was observed in the initial stage of the breakdown of the discharge gap and reached 2–4 MW. Time integration of the pulsed power made it possible to determine the electrical energy that was introduced into the discharge plasma during one sequence of voltage and current pulses. For the conditions of our experiments with metal electrodes in atmospheric pressure air, the maximum energy that was deposited into the plasma in one pulse reached E = 105 mJ (Figure 4).
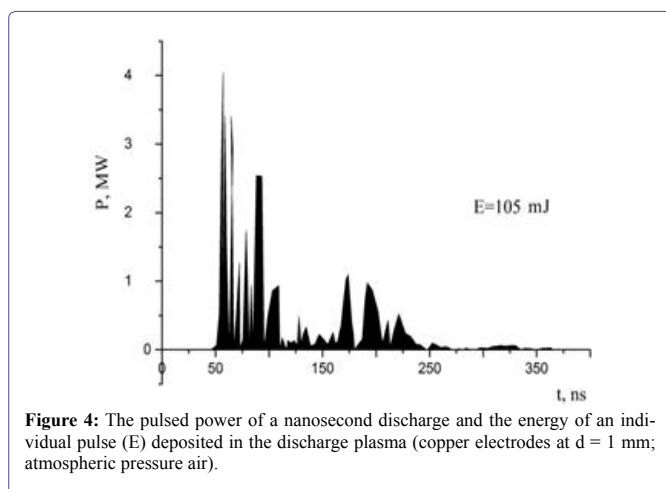

Figure 4: The pulsed power of a nanosecond discharge and the energy of an individual pulse (E) deposited in the discharge plasma (copper electrodes at d = 1 mm; atmospheric pressure air).

The electrical characteristics of the discharge between copper and electrodes in helium are shown in figures 5 and 6. In this case, the maximum amplitude of the negative voltage spike reached 35 kV, and the positive amplitude reached 60 kV, but they were separated by

approximately 20-30 ns in time figure 5. The maximum amplitude of the negative part of the current pulses reached 175 A, and the positive - 150 A figure 5. The maximum value of the pulsed discharge power in helium was observed at a time t = 70-80 ns from the start of the discharge ignition and reached 5.5 MW (Figure 6). The energy that was introduced into the plasma in one discharge pulse was 230 mJ.
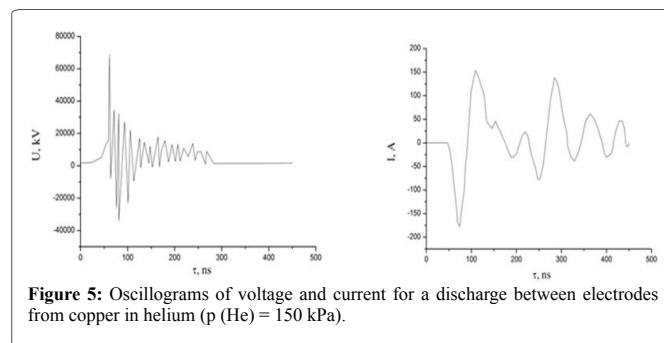

Figure 5: Oscillograms of voltage and current for a discharge between electrodes from copper in helium (p (He) = 150 kPa).
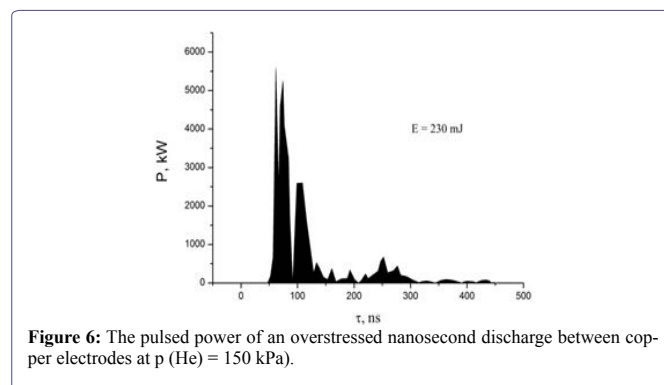

Figure 6: The pulsed power of an overstressed nanosecond discharge between copper electrodes at p (He) = 150 kPa).

The main results of a study of the electrical characteristics of an overstressed nanosecond discharge between chalcopyrite electrodes in argon and nitrogen are shown in figure 7. In this case, the maximum energy input to the plasma per pulse increased significantly: for example, in nitrogen-based mixtures, the energy input reached 375 mJ, and in steam-gas mixtures based on argon, it increased to 440 mJ.
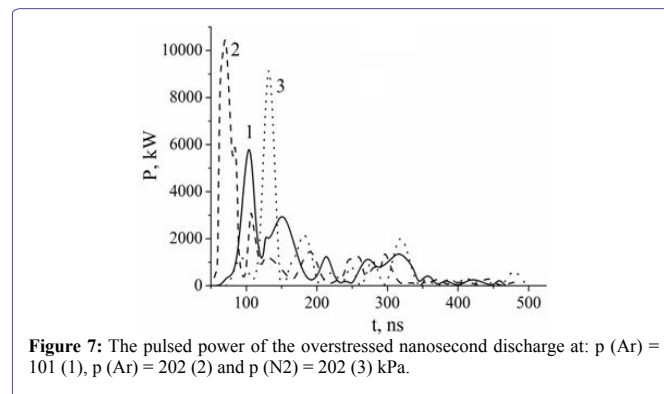

Figure 7: The pulsed power of the overstressed nanosecond discharge at: p (Ar) = 101 (1), p (Ar) = 202 (2) and p (N2) = 202 (3) kPa.

About 90% of the plasma radiation power of an overstressed nanosecond discharge between electrodes of copper, zinc, iron or chalcopyrite, which was emitted in the spectral range of 200-1000 nm, was concentrated in the wavelength range of 200-260 nm.
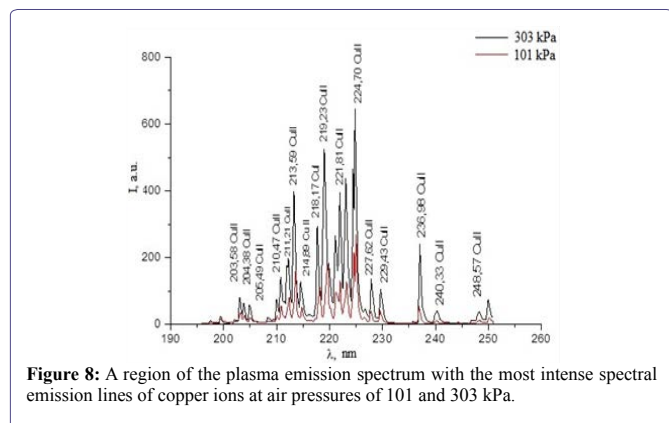
Figure 8: A region of the plasma emission spectrum with the most intense spectral emission lines of copper ions at air pressures of 101 and 303 kPa.

l, nm	Object	I a.u.	Lower level	Upper level
208,41	FeI	100	3d⁶4s²	3d⁵(⁶S)4s24p
224,55	FeII	300	3d⁶(³H)4p	3d⁶(3H)4d
241,78	Fe II	60	3d⁶(³F2)4s	3d⁶(³F2)4p
249,58	Fe I	10000	3d⁷(⁴F)4s	3d⁶(³H)4s4p(³P°)
253,68	Fe II	2000	3d⁶(³H)4s	3d⁶(³H)4p
272,80	Fe I	4000	3d⁷(⁴F)4s	3d⁶(³F2)4s4p(³P°)
309,15	Fe I	120	3d⁷(⁴F)4s	3d⁶(⁵D)4s4p(1P°)

Table 1: Results of decoding the spectrum of the radiation of nanosecond discharge between stainless steel electrodes in air.

In figure 8 the emission spectrum of an overstressed nanosecond discharge between copper electrodes in air is shown. The results of identifying the most intense spectral lines in the radiation spectrum are presented in [19]. An increase in air pressure from 101 to 303 kPa led to an increase in the intensity of all spectral lines in the wavelength range of 200-230 nm. The radiation from copper plasma was dominated by transitions from energy levels of singly charged ions of 8.23-9.12 eV when the electronic configuration of 4p-4s was changed, as well as spectral lines of atoms arising from transitions from highly excited states with energies of 5.68-7.02 eV.

The region with the most intense spectral lines of copper in the wavelength range of 200-230 nm was observed in plasma on a mixture of helium and copper vapor even more pronounced in the emission spectrum of the plasma of an overstressed nanosecond discharge (Figure 9). This region was the main one in the entire UV range of the plasma radiation spectrum: 200–400 nm. Basically, the same spectral lines of copper ions and atoms were observed as in plasma based on a copper-air vapor-gas mixture.
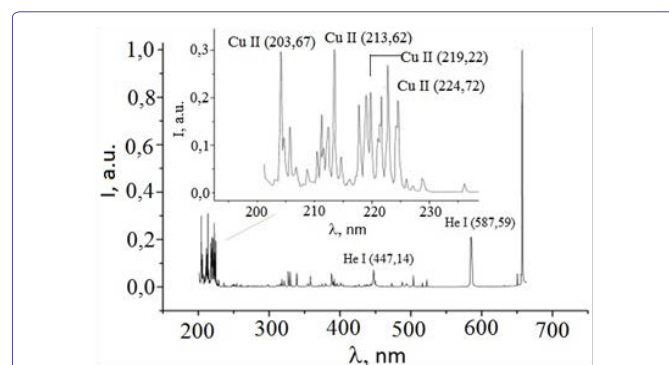

Figure 9: The emission spectrum of a plasma of an overstressed nanosecond discharge in helium at a helium pressure of 150 kPa.

In the ultraviolet radiation spectra of plasma of an overstressed nanosecond discharge between zinc electrodes [20], the most intense were the spectral lines of zinc atoms and ions: 202.6; 206.2 nm Zn II; 250.2; 255.8 nm Zn I. The results of the identification of the main spectral lines of atoms and iron ions that were observed in the discharge between stainless steel electrodes are presented in table 1. The emission spectra of iron plasma are given in [20-22].

The interpretation of the emission spectra of the discharge between the stainless steel electrodes showed that the spectral lines of atoms and singly charged iron ions dominate in such a plasma, and the most intense was the spectral line of 249.6 nm Fe I.

The ultraviolet emission spectra of a plasma of an overstressed nanosecond discharge between chalcopyriteelectrodes in an argon and nitrogen medium are presented in figure 10 and the results of identification of the most intense spectral lines are shown in Tables 2 and 3.

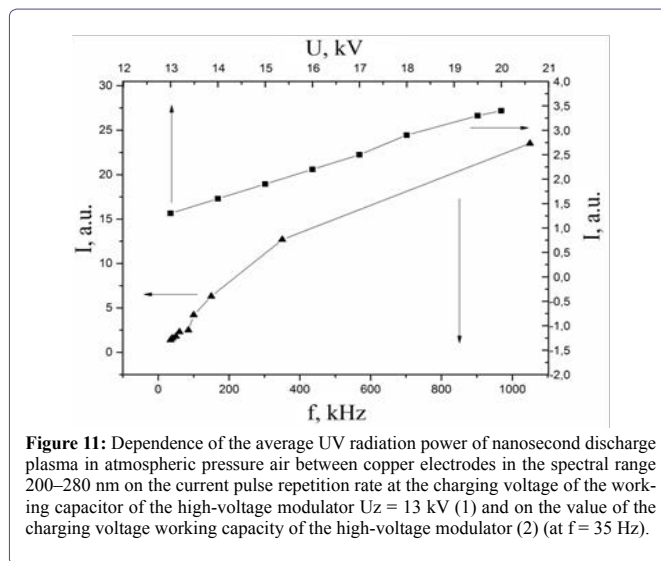| №	λ,nm	I, a.u. (at p(Ar)= 101 kPa)	Object	$E_{low.,}$ eB	$E_{upp.,}$ eB	Lower$_{term}$	Upper$_{term}$
1	218.172	2.26	Cu I	0.00	5.68	4s ²S	4p' ²P°
2	219.95	2.26	CuI	1.39	7.02	4s² ²D	4p" ²D°
3	225.57	0.34	InII	12.68	18.17	5s5d ³D₃	5s4f⁵F°
4	226.37	0.4	CuII	8.92	14.39	4p' ¹F°	4d ³G
5	246.018	0.3	In II	12.68	17.72	5s5d ³D	5s7f⁵F°
6	307.379	1.32	CuI	1.39	5.42	4s² ²D	4p' ²F°
7	328.27	2.13	Cu I	5.15	8.93	4p' ⁴F°	4d' ²G
8	329.05	2.74	Cu I	5.07	8.84	4p' ⁴F°	4d' ⁴F
9	330.79	1.56	Cu I	5.07	8.82	4p' ⁴F°	4d' ⁴G
10	410.17	1.65	In I	-	3.02	5s25p ²P°	5s²6s ²S$_{1/2}$
11	417.83	0.58	Ar II	16.64	19.61	4s ⁴P	4p ⁴D
12	422.26	0.57	Ar II	19.87	22.80	4p ²P°	5s ²P
13	427.75	0.50	Ar II	18.45	21.35	4s' ²D	4p' ²P°
14	436.20	0.32	Ar II	18.66	21.50	3d²D	4p' ²D°
15	451.13	3.1	In I	0.27	3.02	5s²5p ²P°	5s²6s ²S$_{1/2}$

Table 2: The results of the identification of the most intense spectral lines of the products of the destruction of chalcopyrite in an overstressed nanosecond discharge a: p(Ar) = 101 kPa.

As can be seen from figure 10 The main radiation energy of the studied plasma is concentrated in the spectral range of 200-230 nm.
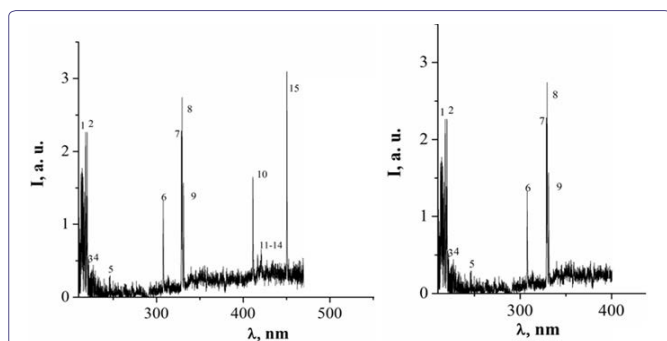
The ultraviolet radiation of chalcopyrite plasma is concentrated mainly on transitions of atoms and ions of copper and indium [10,23]. When studying the optical characteristics of a plasma in the UV region of the spectrum, which was excited by a high-voltage multi-electrode discharge in air (at a pressure p = 101 kPa) between copper electrodes (interelectrode distance d = 1.5 mm), the spectrum of plasma radiation is determined by individual spectral lines [24,25] of atoms and singly charged copper and indium ions, as for a laser plasma, which was formed on the surface of a polycrystalline target from chalcopyrite under vacuum [26,27].

№	λ, nm	I, a.u. (at p(N$_2$)= 101 kPa)	Object	$E_{low.,}$ eB	$E_{upp.,}$ eB	Lower$_{term}$	Upper$_{term}$
1	218.172	2.26	Cu I	0.00	5.68	4s ^{2}S	4p' ^{2}P^o
2	219.95	2.26	CuI	1.39	7.02	4s^2 ^{2}D	4p'' ^{2}D^o
3	225.57	0.34	InII	12.68	18.17	5s5d ^{3}D$_3$	5s4f^{3}F°
4	226.37	0.4	CuII	8.92	14.39	4p' ^{1}F°	4d ^{3}G
5	246.018	0.3	In II	12.68	17.72	5s5d ^{3}D	5s7f^{3}F°
6	307.379	1.32	CuI	1.39	5.42	4s^2 ^{2}D	4p' ^{2}F^o
7	328.27	2.13	Cu I	5.15	8.93	4p' ^{4}F°	4d' ^{2}G
8	329.05	2.74	Cu I	5.07	8.84	4p' ^{4}F°	4d' ^{4}F
9	330.79	1.56	Cu I	5.07	8.82	4p' ^{4}F°	4d' ^{4}G

Table 3: The results of the identification of the most intense spectral lines of the products of the destruction of chalcopyrite in an overstressed nanosecond discharge b: p(N$_2$) = 101 kPa.

Figure 10: The emission spectrum of an overstressed nanosecond discharge between chalcopyrite electrodes at p (Ar) = 101 kPa (limit the spectrum to 200–470 nm, P (N$_2$) = 101 kPa (spectrum limited to 200-400 nm).

Figure 11: Dependence of the average UV radiation power of nanosecond discharge plasma in atmospheric pressure air between copper electrodes in the spectral range 200–280 nm on the current pulse repetition rate at the charging voltage of the working capacitor of the high-voltage modulator Uz = 13 kV (1) and on the value of the charging voltage working capacity of the high-voltage modulator (2) (at f = 35 Hz).

Numerical simulation of plasma parameters

Estimated calculations of some plasma parameters were performed for a low average density of copper vapor (approximately 30 Pa), which is typical for the working medium of low-pressure ion gas discharge lasers using transition metal vapor [31]. The data of Ref. [32] were also taken into account, where the results of studying atmospheric pressure air plasma with a small admixture of copper vapor are also presented at about 30 Pa, which entered the plasma due to erosion of copper electrodes.

At atmospheric pressures of Argon and Helium (p = 152 kPa), a relatively large duration of the leading edge of the voltage pulse (5-7 ns), as well as for a system of electrodes with a weak in homogeneity of the distribution of the electric field strength in the discharge gap, data on the threshold values of the parameter E/N, when runaway of electrons becomes significant, are absent in the literature known to us. Under such experimental conditions, the most probable factor in the preionization of the interelectrode gap is x-ray radiation [33]. In this experiment, a small pulse repetition rate (40-100 Hz) and small-sized autographs on the working surface of the electrodes indicate small average partial discharge pressures of copper vapor in the present experiment. As in [34], traces of erosion had the form of individual points with a diameter of up to 100-200 μm, which relatively evenly filled the working surface of the electrodes. Under the conditions of the present experiment, the maximum value of the E/N parameter reached (at Argon pressure p = 1.5 Atm and d = 1 mm) approximately 1081 Td, and for Helium at the same pressure 811 Td, which is less than the critical value E/N for nitrogen, according to the local criterion for runaway electrons - 1787.7 Td [18,35]. The latest results of numerical simulation of runaway electron generation in atmospheric pressure nitrogen in a needle – plane electrode system showed that this threshold is even higher and is equal to 12120Td [36].

Therefore, for evaluating calculations of atmospheric pressure plasma parameters, we chose the standard software for solving the Boltzmann kinetic equation for the electron energy distribution function (EEDF).

The use of this software assumes a constant electric field in time and space [37]. Under the conditions of our experiment the duration

Figure 11 presents the dependences of the average radiation power of an overstressed nanosecond discharge in the spectral range 200-280 nm via the frequency of the voltage pulses and the magnitude of the charging voltage of the working capacitor of the high-voltage modulator. The frequency dependency of the plasma UV radiation was nonlinear, and the highest growth rate was observed in the frequency range f = 40-350 Hz. With increasing f from 35 to 1000 Hz, the average UV radiation power of an overstressed nanosecond discharge increased by about an order of magnitude. An increase in the charging voltage of the working capacitor from 13 to 20 kV (at f = 35 Hz) led to a twofold increase in the plasma UV radiation power. From the obtained results it is seen that to increase the average power of the UV radiation of the discharge plasma, the most promising is to increase the repetition rate of the exciting voltage pulses.

In pulsed nanosecond discharges in the presence of additives of easily ionized impurities in the form of metal vapors from the material of the electrodes, the plasma electron density can reach 10^{16}-10^{17} cm^{-3} [28]. Therefore, the mechanism of formation of excited metal ions can be determined by the processes of excitation of metal ions in the ground state by electrons, as well as by processes of electron-ion recombination. For these processes involving zinc ions, the effective cross sections are quite large and reach 10^{-16} cm^2 [29,30]. Therefore, it is likely that the excited transition metal ions are formed as a result of the excitation of singly charged metal ions in the ground energy state by electrons and during the dielectronic recombination of doubly charged metal ions with discharge electrons.

of a voltage oscillation in the gap with a half-period of ~ 10 ns and a diffuse discharge, the plasma medium is in an electric field that changes more slowly than the time of establishing the electron distribution function. It is known that the time to establish a quasistationary electron distribution is approximately equal to the relaxation time of the mean electron energy [38,39]

$$\tau = m\upsilon_e \varepsilon \,/\, e^2 E^2$$

Where m - the electron mass, e- the electron charge, E -electric field strength, υ_e - frequency of elastic collisions of electrons with mixture atoms (argon and copper) Estimation of the value of τ for our experiment gives a value of ~ $1 \cdot 10^{-13}$ s, which is much less than the duration of 10 ns. Therefore, we believe that for our experiment we can use the standard software for solving the Boltzmann kinetic equation for the electron energy distribution function, namely Bolsig.

The parameters of the discharge plasma in mixtures of argon and helium with a small addition of copper vapor at atmospheric pressures (component ratio 152 kPa: 30 Pa) were determined numerically and were calculated as total integrals from the EEDF. EEDFs were found numerically by solving the Boltzmann kinetic equation in the two-term approximation. EEDF calculations were performed using the program [22]. Which also includes the effective cross sections for the interaction of electrons with copper atoms in the database of effective cross sections. Based on the EEDFs obtained, a number of plasma parameters are determined depending on the magnitude of the reduced electric field (the ratio of the electric field strength (E) to the total concentration of argon or helium atoms and a small impurity of copper vapor (N)). The parameter variation range E / N = 1-1300 Td ($1 \cdot 10^{-17}$ - $1.3 \cdot 10^{-15}$ V · cm²) for a mixture of copper and argon vapor and E / N = 1-1000 Td for a mixture of copper and helium vapor included the values of the parameter E / N, which were implemented in the experiment. For the vapor-gas mixture Cu: Ar = 30: 152000 at a total pressure of 152.030 kPa, these E / N parameters were equal to 1081 Td and 540 Td Td in the range 0-100 ns and 100 -480 ns, respectively, and for the gas-vapor mixture Cu: He = 30: 152000 at a total pressure of 152.030 kPa, these E / N parameters were equal to 811 Td and 405 Td in the range 0-100 ns and 100-300 ns, respectively (Figure 5). The following processes are taken into account in the integral of collisions of electrons with atoms and molecules: elastic scattering of electrons by copper, argon and helium atoms, excitation of energy levels of copper atoms (threshold energy 1.500 eV, 3.800 eV, 5.100 eV), ionization of copper atoms (threshold energy 7.724 eV); excitation of the energy level of argon atoms (threshold energy 11.50 eV), ionization of argon atoms (threshold energy, 15.80 eV); excitation of the energy level of helium atoms (threshold energy 19.8 eV), ionization of helium atoms (threshold energy, 24.58 eV).

In figure 12 show the dependences of the average electron energy in the plasma of the vapor-gas mixture Cu: Ar = 30: 152000 and Cu: He = 30: 152000 at a total pressure p = 152.030 kPa on the reduced electric field strength.

Mean energy of the discharge electrons for the argon-copper vapor-gas mixture = 152 kPa - 30 Pa increased from 1.583 to 18.45 eV with an increase in the reduced electric field strength from 1 to 1300 Td figure 12 and for the helium-copper mixture = 152 kPa - 30 Pa, it also increased from 0.3818 to 136.3 eV with an increase in the reduced electric field strength from 1 to 1000 Td figure 12 At the same

time, a regularity was observed in the increased rate of its change in the ranges of 1-50 and 1-40 Td for mixtures of the first and second, respectively.

Figure 12: Dependences of the average electron energy in the plasma of the vapor - gas mixture Cu: Ar = 30: 152000 and Cu: He = 30: 152000 at a total pressure p = 152.030 kPa on the reduced electric field strength, respectively.
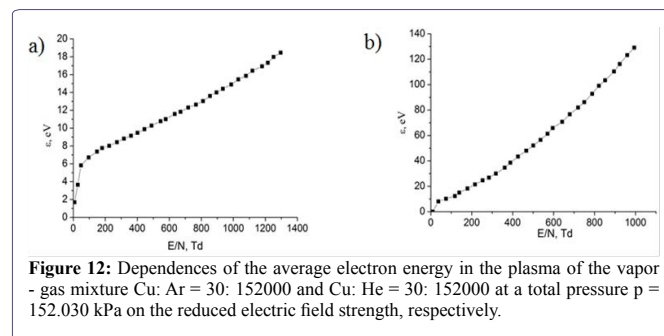
Tables 4 and 5 show the results of calculating the transport characteristics of electrons: Mean energies ε, temperature T K, drift velocity V_{dr} and electron concentration for two mixtures of copper vapor with argon and copper vapor with helium.

E/N, Td	Mixture: Cu - Ar=30 Pa – 152 kPa			
	ε, eV	T⁰K	$V_{dr,}$ m/s	N_e,m⁻³
1	1.583	18362	3.8·10⁶	1.0·10⁺²¹
45	5.786	67118	6.0·10⁵	6.3·10⁺²¹
539	10.66	123656	3.5¹0⁵	1.1·10⁺²²
1076	15.90	184440	6.3·10⁵	8.1·10⁺²¹

Table 4: Transport characteristics of electrons for the mixture Cu - Ar=30 Pa – 152 kPa.

| E/N, Td	Mixture: Cu - He=30 Pa – 152 kPa			
	ε, eV	T⁰K	$V_{dr,}$ m/s	N_e,m⁻³
1	0.382	4431	1.7·10⁶	7.0·10⁺²⁰
35	8.085	93786	9.0·10⁵	1.4·10⁺²¹
414	43.51	504716	1.2·10⁶	1.3·10⁺²¹
828	104.2	1208720	2.4·10⁶	2.6·10⁺²¹

Table 5: Transport characteristics of electrons for the mixture Cu - He=30 Pa – 152 kPa.

For the Cu - Ar mixture = 30 Pa - 152 kPa, the transport characteristics of the electrons are shown in table 4 for the reduced electric field strengths of 1076 Td and 539 Td in the range 0-100 ns and 100 -480 ns, respectively and for the vapor-gas mixture Cu - He = 30 Pa - 152 kPa table 5 they have values for the reduced electric field strengths of 828Td and 414Td in the range 0-100 ns and 100 -300 ns, respectively figure 3 In the second mixture, the mean energies, temperature, and electron drift velocities are much higher than in the first, and the concentration of electrons have higher values in the first mixture table 4.

Figure 13 shows the dependence of specific power losses of the discharge on the processes of collisions of argon and copper atoms with the electrons via the parameter E / N in plasma for the mixture Cu: Ar = 30: 152000 at a total pressure P = 152.030 kPa.

For the reduced field strength E / N = 1076 Td of the mixture of copper vapor with argon, which took place in the range from the

beginning of the breakdown of the interelectrode gap to 100 ns in the first mixture, they did not exceed 23.3% and 38.1%, respectively, and for the reduced field strength E/N = 539 Td, which occurred in the range 100 -480 ns, they had values of 35.7% and 38.2%, respectively. For the second mixture in the time range of 0 -100 ns, 5.3% and 18% for E/N = 828 Td, respectively, and for the reduced field strength E/N = 414 Td, which took place in the range of 100 -300 ns, they had 12.2% and 31.5%, respectively. For copper atoms, they did not exceed 0.09% (for excitation of the resonance state $^2P_{3/2, 1/2}$) for the first mixture at E/N = 1076 Td and 0.28% at E/N = 539 Td, and for the second mixture they did not exceed 0.03% at E/N = 828Td and 0.13% at E/N = 414Td.
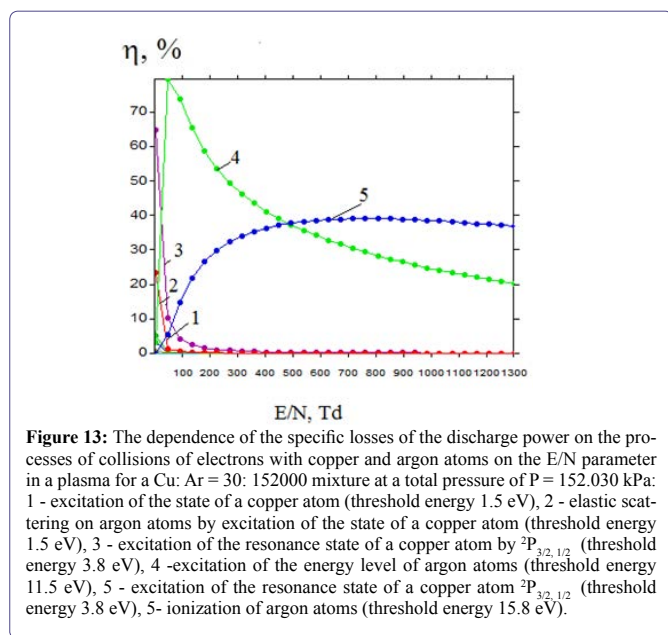
Figure 13: The dependence of the specific losses of the discharge power on the processes of collisions of electrons with copper and argon atoms on the E/N parameter in a plasma for a Cu: Ar = 30: 152000 mixture at a total pressure of P = 152.030 kPa: 1 - excitation of the state of a copper atom (threshold energy 1.5 eV), 2 - elastic scattering on argon atoms by excitation of the state of a copper atom (threshold energy 1.5 eV), 3 - excitation of the resonance state of a copper atom by $^2P_{3/2, 1/2}$ (threshold energy 3.8 eV), 4 -excitation of the energy level of argon atoms (threshold energy 11.5 eV), 5 - excitation of the resonance state of a copper atom $^2P_{3/2, 1/2}$ (threshold energy 3.8 eV), 5- ionization of argon atoms (threshold energy 15.8 eV).

The specific loss of discharge power in a mixture of copper vapor with argon (Argon-Copper = 152 kPa - 30 Pa) for inelastic collisions of electrons with mixture components is maximal for excitation of an energy level with a threshold energy of 11.5 eV argon atoms for a reduced field strength of 45.8 Td figure 13 and for ionizing it with a threshold energy of 15.80 eV for a reduced electric field strength of 807 Td figure 13 they reach 79 % and 39%, respectively. For copper atoms, the specific loss of discharge power in this mixture reaches a maximum value of 64.7% for excitation of the resonance state $^2P_{3/2,1/2}$ at a reduced electric field strength of 1 Td. For the second mixture (He-Copper = 152 kPa - 30 Pa), the specific losses of the discharge power for inelastic collisions of electrons with the mixture components are maximal for excitation of the energy level with a threshold energy of 19.80 eV of helium atoms at a reduced electric field strength of 35.4 Td and for its ionization With a threshold energy of 24.58 eV for a reduced electric field strength of 173 Td and reach 59 % and 40%, respectively. For copper atoms, the specific loss of discharge power in this mixture reaches a maximum value of 13.2% for excitation of the resonance state $^2P_{3/2,1/2v}$ at a reduced electric field strength of 35.4 Td.

For the reduced field strength E / N = 1076 Td of the mixture of copper vapor with argon, which took place in the range from the beginning of the breakdown of the interelectrode gap to 100 ns in

the first mixture, they did not exceed 23.3% and 38.1%, respectively, and for the reduced field strength E/N = 539 Td, which occurred in the range 100 -480 ns, they had values of 35.7% and 38.2%, respectively. For the second mixture in the time range of 0 -100 ns, 5.3% and 18% for E/N = 828 Td, respectively, and for the reduced field strength E/N = 414 Td, which took place in the range 100 -300 ns, they had 12.2% and 31.5%, respectively. For copper atoms, they did not exceed 0.09% (for excitation of the resonance state $^2P_{3/2, 1/2}$) for the first mixture at E/N = 1076 Td and 0.28% at E/N = 539 Td, and for the second mixture they did not exceed 0.03% at E/N = 828Td and 0.13% at E/N = 414Td.

The rate of increase and fall of discharge power losses on the processes of excitation of electronic states and ionization and its values figure 13 is related to the nature of the dependence of the effective cross sections of inelastic collisions of electrons with mixture components on electron energies, their absolute values, and also on the dependence of the electron distribution function on the magnitude of the reduced field strength and threshold energy of the process. The losses in the discharge power due to the excitation and ionization of copper atoms in the range of the reduced electric field strength at which our plasma sources (1076-539 Td) and (828 - 414 Td) operated are small, due to the low content of copper vapor in the mixture.

Tables 6 and 7 shows the highest values of the rate constants of collisions of electrons with copper and argon atoms for the reduced electric field strength, which are a measure of the process efficiency for a mixture of Cu: Ar = 30Pa: 152 kPa, the total pressure of 152030 Pa and a mixture of Cu: He = 30 Pa - 152 kPa, total pressure 152030 Pa. They vary in the range $0.2166 \cdot 10^{-23}$ - $0.1167 \cdot 10^{-11}$ m³/s for characteristic values of the reduced electric field strength. The rate constant of elastic scattering of electrons by copper atoms is maximal and with decreasing values of the reduced electric field strength it decreases 1.99 times for the first mixture, and for the second 1.2 times. The excitation rate constant of the resonance state of copper for the second mixture is higher and has values of $0.9415 \cdot 10^{-12}$ and $0.7146 \cdot 10^{-12}$ m³/s for the reduced electric field strength at which the plasma source of film deposition works (E/N = 414 Td and E / N = 828 Td).

| N	Process	k, m³/s	E/N=1 Td	E/N=45 Td	E/N=539Td	E/N=1076Td
1	Cu Elastic	k1	0.5851E-12	0.8009E-12	0.1109E-11	0.1167E-11
2	Ar Effective (momentum)	k2	0.1947E-13	0.1258E-12	0.2081E-12	0.2365E-12
3	Cu Excitation 3.80 eV	k3	0.6046E-14	0.2987E-12	0.6848E-12	0.8569E-12
4	Ar Excitation 11.50 eV	k4	0.1893E-19	0.1501E-15	0.5766E-14	0.1371E-13
5	Ar Ionization 15.80 eV	k5	0.2166E-23	0.7494E-17	0.4492E-14	0.1634E-13

Table 6: Values of the rate constants of electron collisions with copper and argon atoms for the a: mixture: Cu - Ar = 30 Pa - 152 kPa.

Characteristics of thin films based on nanostructures of transition metal oxides and chalcopyrite

The most characteristic results of the study of the optical characteristics of nanostructures based on transition metal oxides and chalcopyrite, which were deposited on a glass substrate installed near the discharge gap, are shown in figures 14-17.

N	Process	k, m³/s	E/N=1 Td	E/N=45 Td	E/N=539Td	E/N=1076Td
1	Cu Elastic	k1	0.8448E-12	0.9477E-12	0.1139E-11	0.1022E-11
2	He Effective (momentum)	k2	0.2181E-13	0.7707E-13	0.6115E-13	0.5188E-13
3	Cu Excitation 3.80 eV	k3	0.2198E-19	0.4941E-12	0.9415E-12	0.7146E-12
4	He Excitation 19.80 eV	k4	0.000	0.8347E-16	0.3250E-14	0.5316E-14
5	He Ionization 24.58 eV	k5	0.000	0.1679E-16	0.6732E-14	0.1469E-13

Table 7: Values of the rate constants of electron collisions with copper and argon atoms for the b: mixture: Cu - He = 30 Pa - 152 kPa.
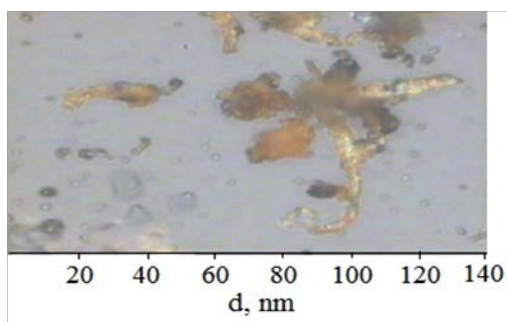
Figure 14: The surface structure of the film obtained from the sputtering products of copper electrodes in atmospheric pressure air for 30 minutes under the influence of an overstressed nanosecond discharge (f = 100 Hz).
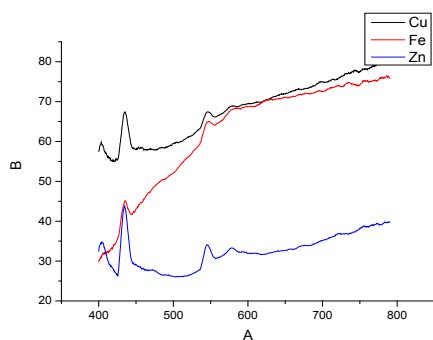
Figure 15: Radiation transmission spectrum of thin films synthesized by sputtering electrodes of copper, stainless steel and zinc in the air of atmospheric pressure for 30 minutes (center of the substrate, f= 100 Hz).

Figure 14 presents an image of the surface of a film obtained from the erosion products of copper electrodes and the products of dissociation of air molecules in an overstressed nanosecond discharge. The optical characteristics of nanostructured films were studied at an interelectrode distance of 1 mm. To determine the sizes of nanostructures, a gel was applied on the film surface based on standard spherical gold nanostructures with a diameter of 20 nm (which are highlighted in yellow in image) (Figure 14). A comparative analysis of the sizes of spherical gold nanostructures and transition metal oxide nanostructures showed that the sizes of synthesized copper oxide

nanostructures are in the range of 2–20 nm. The transverse sizes of nanostructures based on zinc and iron oxides were in the range of 2–50 nm.
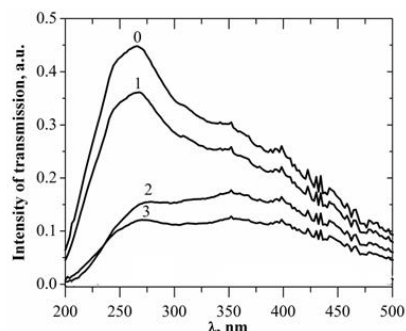
Figure 16: Transmission spectra of samples of chalcopyrite films deposited on quartz substrates depending on pressure and type of gas medium: 0 - without sample;1 - pure quartz glass;2 - electrodes with CuInSe$_2$ at p (Ar) = 13.3 kPa;3 - CuInSe$_2$ at p (Ar) = 101 kPa.
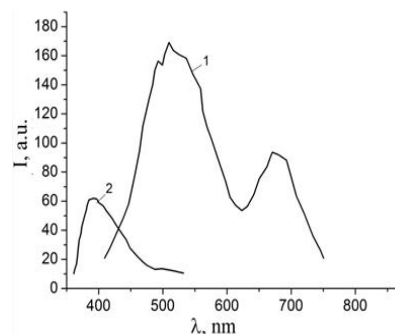
Figure 17: Photoluminescence spectra of a thin film synthesized by sputtering zinc electrodes in a nanosecond discharge in atmospheric pressure air, obtained upon excitation by radiation with a mercury lamp at wavelengths of 270 (1) and 330 (2) nm.

Figure 15 presents the transmission spectra in the visible region by film nanostructures of transition metal oxides. The transmission of these films increased with increasing wavelength. The transmission spectra had the form of continua with narrow enlightenment bands. The transmission spectrum of the film of copper oxide correlates well with the spectrum of the transmission of copper oxide (Cu$_2$O) nanostructures [23,40]. Narrow bands of enlightenment of films in the blue region of the spectrum (at wavelengths of 420 and 450 nm) can be associated with the action of ultraviolet radiation from the discharge in the spectral range 200-230 nm on the film during its synthesis. The same enlightenment bands were observed for films based on zinc oxide. The cause of the appearance of such enlightenment bands may be radiation defects of films of copper and zinc oxides, as well as the formation of new energy levels in these compounds. The most intense were the transmission bands of films based on zinc and copper oxides, which correlated with selective and intense plasma radiation of zinc and copper vapors in the spectral range of 200-230 nm. For a nanosecond discharge between stainless steel electrodes, the selectivity and intensity of plasma radiation decreases, which leads to a decrease in the intensity of the transmission bands for films of iron oxides.

In figure 16 the radiation transmission spectrum of chalcopyrite films, synthesized in plasma based on argon, and obtained by transillumination of films by deuterium lamp radiation. The strongest absorption of radiation of the deuterium lamp by chalcopyrite films was observed during their synthesis in the high-pressure argon and is mainly due to the fact that in the process of chalcopyrite films deposition, they repeat the stoichiometry of electrodes. Other possible reason of strong absorption is an increase in the thickness of the chalcopyrite film at atmospheric pressure of argon, which is due to the increase in discharge current and energy contribution to plasma. The main features of transmission spectra of chalcopyrite films at different pressures of argon remained unchanged when replacing the deuterium lamp with thermal, which allowed carrying out research in the spectral range of 400-800 nm.

The photoluminescence spectra of zinc oxide-based nanostructures at excitation wavelengths in the range 270–550 nm are shown in figure 17. Photoluminescence of the studied nanostructures was most effective under the action of radiation with a wavelength of 330 nm. Photoluminescence of nanostructures in the UV region was practically absent and in the red region, it was characterized by two broad maxima in the wavelength ranges of 450–480 nm and 650–680 nm. As the luminescence excitation wavelength increased to the visible spectral region (up to 550 nm), the photoluminescence spectra also shifted to the long-wavelength region, and the photoluminescence intensity decreased significantly. With a decrease in the luminescence excitation wavelength from 330 to 270 nm, the luminescence intensity decreased most significantly for the green and red bands.

The photoluminescence spectra of nanostructured films based on copper oxide are given in [9]. Such nanostructures were most efficiently excited by radiation with a wavelength of 330 nm. These photoluminescence spectra were characterized by two broad maxima in the spectral range of 400-600 nm, which have been shifted to the long-wavelength region of the spectrum and decreased in intensity upon transition from the wavelength of the exciting radiation at 330 nm to both the region of 270 nm and the region of 380 nm. It was established in [12-41] that, when the growth of transparent conducting balls based on zinc oxide nanostructures was assisted by the UV radiation of a mercury lamp, it contributed to the improvement of their electrical characteristics due to the formation of additional donor centers and the reduction of charge carrier scattering at the grain boundaries of nanowhiskers. In our case, there is no need to use an external source of UV radiation, since the studied plasma itself is a selective emitter in the spectral range of 200-230 nm.

Conclusion

It was shown that an overstressed nanosecond discharge in air, nitrogen, and argon at atmospheric pressures between electrodes of transition metals (Zn, Cu, Fe), as well as chalcopyrite (CuInSe$_2$) is a selective point source of emission of atoms and ions of zinc, copper and iron in the spectral range 200-250 nm. Numerical simulation of plasma parameters revealed that the loss of discharge power due to the excitation and ionization of copper atoms in the range of reduced electric field strengths at which our plasma sources (1076-539 Td) and (828 - 414 Td) operated was small, due to the low content of copper vapor in the mixture. Simultaneously with the radiation, the discharge plasma is a source of flows of nanostructures of transition metal oxides and chalcopyrite, which can be used for applications in microbiology, medicine and agricultural technologies, as well as in micro-nanotechnologies and optoelectronics.

References

1. Vasilyak LM (2009) The use of pulsed electric discharge lamps for bactericidal treatment. Electrical processes in engineering and chemistry 45: 30.

2. Shuaibov OK, Grabova IA, Shevera IV (2018) Gas-discharge UV-VUV exciplex and low-pressure halogen lamps. Monograph, (Uzhgorod National University), Ukraine.

3. Shuaibov OK, Malinina AA, Malinin AN (2019) New gas-discharge methods for producing selective ultraviolet and visible radiation and synthesis of transition metal oxide nanostructures. Monograph.

4. Egorova EM (2014) Biological effects of metal nanoparticles.

5. Benedikt J, Hansen O, Polonskyi O, Hefny MM, Necas D, et al. (2019) Atmospheric Plasmas for Generation of nanostructured Materials. In: Proceedings of SAPP XX11 22 nd Symposium on Application of Plasma rocesses and 11th EU – Japan Joint Symposium on Plasma Processing, edited Medvecka V, Orzagh J, Papp P, Vatejcik S(eds.), 152-154.

6. Malinina A, Malinin A, Shuaibov A (2019) Emission Chacteristics of Cas-Discharge Plasma of Atmospheric Pressure Dielectric Barrier Discharge on Zinc Diodide Vapor wich Neon and Xenon Mixtures. In; Proceedings of SAPP XX11 22 ndSymposium on Application of Plasma Processes and 11th EU - Japan Joint Symposium on Plasma Processing, edited Medvecka V, Orzagh J, Papp P, Vatejcik Pg nos: 156-164.

7. Popovich GB, Malinina AA (2019) The formation of seedlings of lettuce and cabbage under theinfluence ofadditionallighting. Crop production and soil science 10: 58.

8. Shuaibov OK, Minya OI, Gomoki ZT, Daniil VV (2017) Method for nanostructuring a glass surface in atmospheric pressure air. Ukraine patent for utility model.

9. Shuaibov A, Minya A, Malinina A, Golomb R, Shevera I, et al. (2018) Synthesis of nanostructured transition metal oxides by a nanosecond discharge in air with assistance of the deposition process by plasma UV-radiation. Advances in Natural Sciences: Nanoscience and Nanotechnology 9: 035018.

10. Shuaibov AK, Minya AY, Gomoki ZT, Hrytsak RV, Malinina AA, et al. (2019) Spectroscopic Study of the Decomposition of a Chalcopirite Molecule in a Overstressed Nanosecond Discharge on a Mixture of Nitrogen with CuInSe$_2$ Vapor Compound. Journal of Physics and Chemistry Reseach.

11. Shuaibov O, Chyhin V, Malinina A, Danilo V (2019) Sourse of bacteriocidic ultra-violet radiation and flow of nano-particles of Zinc and Copper oxide for applications in Microbiology. Mtdicine and Nanotechnology, Bulletin of the Khmelnitsky National University. Technical science 4: 209.

12. Zatolokin VD, Moshkin AS (2010) the effect of aqueous dispersions of oxide metal nanostructures on the course of purulent wounds. Bulletin of experimental and clinical surgery 3: 44.

13. Shoot VN, Mozhzharov SE, Yanchenko VV (2016) Physical and antibacterial properties of ultrafine copper powders, Chemical technology and ecology. Bulletin of Vitebsk State Technological University31: 97.

14. Chung SH, Hoffman A, Bader SD, Liu C, Kay B, et al. (2004) Biological sensors based on Brownian relaxation of magnetic nanoparticles. Appl. Phys. Lett 85: 14,2971.

15. Shuaibov AK, Minya AY, Gomoki ZT, Danilo VV, Pinzenik RV (2018) Characteristics of a high-current pulsed discharge in air with an ectonic mechanism for the injection of copper vapor into a discharge gap. Electrical processes in engineering and chemistry 54: 46.

16. Mesyat GA (1995) Ecton or electron avalanche frommetal. Usp. Fizich. Nauk 38: 567-590.

17. Babich LP (2003) High-Energy Phenomena in Electric Discharges in Dence Gases. Theory, Experiment and Natural Phenomena. (Futurepast, Arlington. Virginia: ITS Science and Technology Series,).

18. TarasenkoVF (2014) Runaway electrons preionized diffuse discharge.

19. ShuaibovAK, MinyaAY, MalininaAA, MalininAN, DaniloVV (2018) Synthesis of Copper Oxides Nanostructures by an Overstressed Nanosecond Discharge in Atmospheric Pressure Air between Copper Electrodes. American Journal of Mechanical and Materials Engineering 2: 8-14.

20. Shuaibov OK, Minya OY, Chuchman MP, Malinina AA, Malinin AN (2018) Parameters of Nanosecond Overvoltage Discharge Pla sma in a Narrow Air Gap between the Electrodes Containing Electrode Material Vapor. UkrJPhys 63: 790-801.

21. Shuaibov OK, Minya OY, Gomoki ZT, Danilo VV (2016) Windowless, spot, ultraviolet lamp. Ukraine patent for utility model.21: 6.

22. Shuaibov A, Mynia O, Chuchman M, Homoki Z, Danylo V (2017) Characteristics of overstrained nanosecond discharge in a mixture of air wich copper steam. In: Proceedings of the XIII International Conference "Electronics and Applied Physics", Taras Shevchenko National University Kyiv, Ukraine. Pg no: 151-152.

23. Hrytsak RV, Malinina AO, Minya OJ, Shuaibov OK, Neymet SY (2019) Characteristics of overstressed nanosecond discharge between electrodes from chalcopirite in argon of atmospheric pressure. In; Abstracts of XIX-International Young Scientists Conferenceon Applied Physics, Taras Shevchenko National University, Kyiv, Ukraine. Pg nos: 37-38.

24. Anpilov AM, Barkhudarov EM, Kozlov YUN, Kossyi IA, Misakyan MA, et al. (2019) UV Radiation of High-Pressure Multi-Electrode Surface Discharge in Gaseous Medium, Plasma Physics Reports 45: 268.

25. Kacher IE, Shuaibov AK, Rigan MYU, Dashchenko AI (2002) Optical Diagnostics of Laser Evaporation of $CuInS_2$ Polycrystalline Compound. High Temperature 40: 814-817.

26. Shuaibov OK, Chuchman MP, Shimon LL, Kacher IE (2003) Investigation of Optical Characteristics and Parameters of Laser Plasma of $CuInS_2$ Polycrystalline Batch and its Components. Ukrainian Journal of Physics 48: 223.

27. Shuaibov AK, Chuchman MP, Dashchenko AI (2003) Investigation of the dynamics of radiation of an erosive laser plasma of a $CuInS_2$ polycrystal. JETP Letters 29: 23.

28. Levko D, Raja LL (2016) Early stage time evolution of a dense nanosecond micro discharge use in fast switching applications. Physics of Plasmas 22: 123518.

29. Gomonai AN (2015) Radiative Decay np^2 autoionization States under dielectronic Recombination of the Zn^- and Cd^- Ions. Journal of Applied Spectroscopy 82: 13-18.

30. Ovcharenko EV, Imre AI, Gomonai AN, Hutych YUI (2010) Emission cross-sections of the In^{2-} ion VUV laser transitions at electron–In^+ ion collisions. J Phys B Atom. Mol Opt Phys 43: 230.

31. Ivanov IG (1984) Metal vapor lasers with transverse discharge types. Avtometriya 1: 19.

32. Pashchina AS, Efimov AV, Chinnov VF (2017) Optical studies of multi-component plasma of a capillary discharge. Supersonic expiration mode. High temperature 55: 669.

33. Bakst AG, Burachenko AG, Lomaev MI, Panchenko AN, Tarasenko VF (2015) A source of periodic pulsed UV radiation based on a volume discharge initiated in nitrogen by a beam of electron avalanches. Quantum Electronics 45: 366-370.

34. Karelin VI, Trenkin AA, Shibitov YUM, Blinova OM, Yasnikov IS (2017) Microstructure of the areas where a spark discharge affects the surface of a flat copper electrode in air in the tip-plane gap. Journal of Technical Physics 87: 1411.

35. Tarasenko VF, Yakovlenko SI (2004) The mechanism of runaway of electrons in dense gases and the formation of powerful subnanosecond electron beams. Physics Uspechi 1749: 53.

36. Kozhevnikov YUV, Kozyrev AV, Dmitrieva NM (2014) Theoretical 0-D modeling of a subnanosecond high-pressure gas discharge. News of Higher Educational Establishments Physics 57: 130.

37. http://www.bolsig.laplace.univ-tlse.fr.

38. Reiser YUP (1987) Physics of gas discharge.

39. Mkrtchyan MM, Platonenko VT (1979) Kinetics of a gas-discharge XeF excimer laser. Soviet Journal of Quantum Electronics 9: 967.

40. Zamanova EN, Alieva LA (2008) Structure and optical properties of films of copper oxide Cu_2O obtained by low-temperature chemical deposition. Fizika XIV.

41. Abduev AKh, Asvarov ASh, Akhmetov AK, Emirov RM, Belyaev VV (2017) UV-assisted growth of transparent conductive layers based on zinc oxide. JETP Letters 43.